A Modified Method of Fundamental Solutions with Source on the Boundary for Solving Laplace Equations with Circular and Arbitrary Domains

D.L. Young[1] , K.H. Chen[2], J.T. Chen[3] and J.H. Kao[4]

Abstract: A boundary-type method for solving the Laplace problems using the modified method of fundamental solutions (MMFS) is proposed. The present method (MMFS) implements the singular fundamental solutions to evaluate the solutions, and it can locate the source points on the real boundary as contrasted to the conventional MFS, where a fictitious boundary is needed to avoid the singularity of diagonal term of influence matrices. The diagonal term of influence matrices for arbitrary domain can be novelly determined by relating the MFS with the indirect BEM and are also solved for circular domain analytically by using separable kernels and circulants. The major difficulty of the coincidence of the source and collocation points in the conventional MFS is thereby overcome. The off-diagonal coefficients of influence matrices can be easily determined by using the two-point function. The ill-posed nature of the conventional MFS then disappears.

Finally, we provide numerical evidences that the present method improves the accuracy of the solution after comparing with the conventional MFS, in particular for complicated boundaries in which the conventional MFS may encounter difficulties. Good agreements are observed as comparing with analytic or other numerical solutions.

Keyword: Conventional MFS, MMFS, indirect BEM, generalized indirect BEM, singular fundamental solution, off-set boundary, fictitious boundary, discontinuous B. C., circulants.

1 Introduction

Because of the trend in the fast development of computer, numerical methods play an important role in solving realistic engineering problems especially when the geometry is complex and an exact solution for the pertinent real world problem is not available. In scientific computing realm of numerical methods of the developed finite difference method (FDM) and finite element method (FEM), mesh generation of a complicated geometry is always the most time consuming part of the solution process in the stage of model development for engineers in dealing with the engineering and science problems, particularly in 3-D case, because those methods require approximations to be made throughout the interesting domain.

Boundary element method (BEM) is essential to discretize the boundary only instead of the domain, which takes a little time for one-dimension reduction in mesh generation. Due to its unique feature of mesh reduction, the BEM has become a major numerical method for solving various kinds of multi-dimensional problems with the complicated domain.

The BEM is necessary to discretize the boundary only for one-dimension reduction in contrast with the domain methods of FEM or FDM. From the viewpoint of mesh reduction method, the BEM can be viewed as the first generation of mesh reduction method and it has attracted great attention from science and engineering communities. Although significant mesh reduction has been gained, the BEM still has inconvenience in irregular surface boundary for 3-D problem (Nishimura

[1] Corresponding author. Tel.: +886-2-2362-6114; E-mail address: dlyoung@ntu.edu.tw. Distinguished Professor, Department of Civil Engineering, National Taiwan University, Taipei, Taiwan.

[2] Assistant Professor, Department of Information Management, Toko University, Chia-Yi**,** Taiwan.

[3] Distinguished Professor, Department of Harbor and River Engineering, National Taiwan Ocean University, Keeling, Taiwan.

[4] Graduate student, Department of Harbor and River Engineering, National Taiwan Ocean University, Keeling, Taiwan.

2002). For the first generation of mesh reduction method, the BEM proposed a simple technique for obtaining the principal values in the singular and hypersingular equations (Chen & Hong 1992; Hadamard 1952; Tanaka *et al.* 1994). Some efficient methods were provided by employing the adaptive mesh scheme and the FMM to improve the efficiency of the dual BEM (Chen *et al.* 2002c, 2004b; Kita & Kamiya 1994; Nishimura 2002; Rokhlin 1983; Stewart & Hughes 1997) for solving 2-D acoustics and water wave problems.

In recent years, science and engineering communities have paid attention to the meshless method in which the element is free (Atluri *et al.* 2006). The meshless method is the mesh reduction method that no mesh is required and only boundary nodes are necessary. From the viewpoint of mesh reduction method, the meshless method can be seen as the second generation of mesh reduction method. The second generation of mesh reduction technique possesses a great promise to replace the FEM and BEM as a dominant numerical method. Because of neither domain nor surface meshing required for the meshless method, it is very attractive for engineers in model creation. The initial idea of meshless method dates back to the smooth particle hydrodynamics (SPH) method for modeling astrophysical phenomena (Gingold & Maraghan 1977). Several meshless methods have also been reported in the literature, for example, the element-free Galerkin method (Belytschko *et al.* 1994) and the reproducing kernel method (Liu *et al.* 1995).

The MFS has been employed to solve some engineering problems (Balakrishnan & Ramachandran 2000; Chen *et al.* 1998; Cheng *et al.* 2000; Tsai *et al.* 2002; Young & Ruan 2005). Since only boundary nodes are distributed, it is a kind of meshless method. A comprehensive review of the MFS was given by Fairweather & Karageophis 1998. The source points are distributed on the fictitious boundary (nonphysical boundary). Besides, the kernel function is composed of two-point function which is a kind of the radial basis function. By distributing single or double layer potentials on the fictitious boundary, the solution can be solved. A regular formulation and

singularity-free method were obtained. Also, a meshless formulation can be achieved. The MFS is easy to learn, to use and to program and has high order of accuracy. It seems that this method is very attractive. However, the MFS has not become a popular numerical method because of the controversial artificial boundary (off-set boundary) outside the physical domain. The off-set boundary distance is difficult to decide in general for real engineering problems with a complicated geometry. The diagonal coefficients of influence matrices become singular in common case when the off-set boundary approaches to the real boundary. The influence matrices are ill-posed when the off-set boundary is far away from the real boundary. It results in an ill-posed problem since the condition number for the influence matrix is very large. The location of source and observation points is vital to the accuracy of the solution by using the conventional MFS. Until now, no objective criterion to select the optimal source location has been developed in spite of a large amount of numerical experiments.

Recently, an improved technique which is the so called as boundary knot method or boundary collocation method was introduced by Chen and his collaborators (Chen & Tanaka 2002; Chen & Hon 2003), Kang and his coworkers (Kang e*t al.* 1999; Kang & Lee 2000) as well as Chen and his coworkers (Chen *et al.* 2000, 2002a, 2002b, 2004a). The method has overcome the drawback of ambiguous off-set boundary due to employing the nonsingular general solutions instead of the singular fundamental solutions to solve this trouble issue. In these references, the method only works well in regular geometry with the Dirichlet and Neumann boundary conditions (B. Cs.). Even though this method can locate the source points on the physical boundary and has the non-singular kernels, it still results in the ill-posed matrices.

Therefore, a MMFS for solving the Laplace problems is proposed based on the potential theory. The source points and collocation points are located on the real boundary to avoid the difficulty in selecting the source location by using special treatment of singularity. The present method is to distribute the observation and source points on

the coincident locations of the real boundary. Because the MFS is similar to the indirect BEM, it is one kind of regular BEM instead of the difference of lumped source and distributed source. The method can be treated as a special case of the indirect BEM. The finite value of the diagonal terms of the influence matrices can be extracted out by relating the MFS with the indirect BEM and can also be derived by using separable kernels and circulants analytically. The off-diagonal coefficients of influence matrices can be easily determined by the two-point function. Finally, the program of the new meshless method (MMFS) for solving the Laplace problems subject to the various types of B. C. is developed.

2 Formulation of MMFS

The governing equation for the Laplace problem is shown as follows:

$$\nabla^2 u(x) = 0, \quad x \in D, \tag{1}$$

where ∇^2 is the Laplacian operator, D is the domain of the problem. The boundary conditions are shown as follows:

$$u(x) = \overline{u}, \quad x \text{ on } B_1 \tag{2}$$
$$t(x) = \overline{t}, \quad x \text{ on } B_2 \tag{3}$$

where $t(x) = \partial u(x)/\partial n_x$ and B_1 is the essential boundary (Dirichlet boundary) in which the potential is prescribed, B_2 is the natural boundary (Neumann boundary) where the normal derivative of the potential in the n_x direction is specified, and B_1 and B_2 construct the whole boundary of the domain D. By using the MMFS, the representation for the solution can be expressed in terms of the strengths of the singularities (s^j) as

(i) *UL* method

$$u(x^i) = \sum_{j=1}^{2N} \ln(r_{ij}) A_j = \sum_{j=1}^{2N} U_{ij} A_j$$
$$t(x^i) = \sum_{j=1}^{2N} \frac{y_k \overline{n_k}}{r_{ij}^2} A_j = \sum_{j=1}^{2N} L_{ij} A_j \tag{4}$$

where x^i is the ith collocation point. A_j is the jth generalized unknown using the *UL*

method, $r_{ij} = \left| s^j - x^i \right|$, in which, s^j is the jth source point, n_k is the kth component of the outward normal vector at s; $\overline{n_k}$ is the kth component of the outward normal vector at x and $y_k \equiv x_k - s_k$, and $2N$ is the number of the distributed source nodes.

(ii) *TM* method

$$u(x^i) = \sum_{j=1}^{2N} \frac{y_k n_k}{r_{ij}^2} C_j = \sum_{j=1}^{2N} T_{ij} C_j,$$
$$t(x^i) = \sum_{j=1}^{2N} (2\frac{y_k y_l n_k \overline{n_l}}{r_{ij}^4} - \frac{n_k \overline{n_k}}{r_{ij}^2}) C_j = \sum_{j=1}^{2N} M_{ij} C_j,$$
$$\tag{5}$$

where C_j is the jth generalized unknowns using the *TM* method.

To desingularize the kernels, singularity, s is shifted to on the off-set (auxiliary) boundary (B') away from the real boundary (B). This method is termed the conventional MFS. However, it encounters the ill-posed influence matrix. The off-set distance between B and B' needs to be chosen deliberately. To overcome the drawback of ambiguous off-set boundary of the ill-posed problem, s^j is distributed on the real boundary by using the proposed technique to overcome the singularity of the kernels. This method is called the MMFS.

From the mathematical point of view, the MMFS is equivalent to the indirect BEM and it can be viewed as a discrete version of the indirect BEM instead of the difference of lumped source and distributed source. The method can be treated as a special case of the indirect BEM. Therefore, the indirect BEM can provide us useful information for determining the diagonal terms of the influence matrices. Based on the potential theory for the indirect BEM, we have two kinds of formulation

(i) *UL* method (single-layer potential approach)
The field solution in terms of the single-layer potential approach of the indirect BEM is

represented as

$$u(x) = \int_B U(s,x)\phi(s)dB(s), \tag{6}$$

$$t(x) = \int_B L(s,x)\phi(s)dB(s), \tag{7}$$

where u and t are the potential and its normal derivative, x and s denote the field point and source point, respectively, ϕ is the generalized unknown density function for the single-layer potential and

$$U(s,x) = \ln(r_{ij}), \tag{8}$$

$$L(s,x) = \frac{\partial U(s,x)}{\partial n_x} = \frac{y_i \overline{n_i}}{r_{ij}^2}, \tag{9}$$

for the 2-D Laplace problem, in which $r \equiv |s^j - x^i|$ is the distance between the source (s) and collocation points (x).

(ii) *TM* method (double-layer potential approach)

The double-layer potential approach is expressed as

$$u(x) = \int_B T(s,x)\varphi(s)dB(s),$$
$$t(x) = \int_B M(s,x)\varphi(s)dB(s), \tag{10}$$

where φ is the generalized unknown density function for the double-layer potential and

$$T(s,x) = \frac{\partial U(s,x)}{\partial n_s} = \frac{y_i n_i}{r_{ij}^2}, \tag{11}$$

$$M(s,x) = \frac{\partial^2 U(s,x)}{\partial n_s \partial n_x} = 2\frac{y_i y_j n_i \overline{n_j}}{r_{ij}^4} - \frac{n_i \overline{n_i}}{r_{ij}^2}. \tag{12}$$

To avoid the singularity of the kernels, s^j are distributed on B' in a similar way of the conventional MFS. However, it will encounter the ill-posed influence matrix. This method is termed the generalized indirect BEM. To overcome the drawback of ambiguous off-set boundary of the ill-posed problem, s is distributed on the real boundary by regularizing the singular integrals. Many researchers have paid attention to regularization

techniques for singular and hypersingular integrals to ensure a finite value (Principal value). This method is called the indirect BEM.

By superimposing $2N$ constant source distribution, ϕ or φ (or concentrated strength, A_j or C_j) along the off-set boundary and collocating the $2N$ points on the real boundary, we have

$$[U_{ij}] = \begin{bmatrix} a_{1,1} & \cdots & a_{1,2N-1} & a_{1,2N} \\ a_{2,1} & \cdots & a_{2,2N-1} & a_{2,2N} \\ \vdots & \ddots & \vdots & \vdots \\ a_{2N,1} & \cdots & a_{2N,2N-1} & a_{2N,2N} \end{bmatrix}, \tag{13}$$

$$[L_{ij}] = \begin{bmatrix} b_{1,1} & \cdots & b_{1,2N-1} & b_{1,2N} \\ b_{2,1} & \cdots & b_{2,2N-1} & b_{2,2N} \\ \vdots & \ddots & \vdots & \vdots \\ b_{2N,1} & \cdots & b_{2N,2N-1} & b_{2N,2N} \end{bmatrix}, \tag{14}$$

$$[T_{ij}] = \begin{bmatrix} c_{1,1} & \cdots & c_{1,2N-1} & c_{1,2N} \\ c_{2,1} & \cdots & c_{2,2N-1} & c_{2,2N} \\ \vdots & \ddots & \vdots & \vdots \\ c_{2N,1} & \cdots & c_{2N,2N-1} & c_{2N,2N} \end{bmatrix}, \tag{15}$$

$$[M_{ij}] = \begin{bmatrix} d_{1,1} & \cdots & d_{1,2N-1} & d_{1,2N} \\ d_{2,1} & \cdots & d_{2,2N-1} & d_{2,2N} \\ \vdots & \ddots & \vdots & \vdots \\ d_{2N,1} & \cdots & d_{2N,2N-1} & d_{2N,2N} \end{bmatrix}, \tag{16}$$

where the elements can be obtained by

$$a_{i,j} = U_{ij}\rho(j), \quad j = 1,2,3,\cdots,2N, \tag{17}$$
$$b_{i,j} = L_{ij}\rho(j), \quad j = 1,2,3,\cdots,2N, \tag{18}$$
$$c_{i,j} = T_{ij}\rho(j), \quad j = 1,2,3,\cdots,2N, \tag{19}$$
$$d_{i,j} = M_{ij}\rho(j), \quad j = 1,2,3,\cdots,2N, \tag{20}$$

in which

$$\rho(j) = \begin{cases} \rho_j, & \text{for the indirect BEM}, \\ 1, & \text{for the MMFS}, \end{cases} \tag{21}$$

where ρ_j is a set of integral weights of the indirect BEM. For the MMFS, $\rho(j)$ is reduced to one since source distribution is lumped on the concentrated point.

3 An analytical derivation of diagonal coefficients of influence matrices with circular domain for MMFS

By adopting the addition theorem, the four kernels in the dual formulation are expanded into de-

generate kernels which separate the field point, x, and source point, s, as follows (Abramowitz 1972):

$$U(s,x) = \ln r =$$
$$\sqrt{(\rho\cos(\phi) - R\cos(\theta))^2 + (\rho\sin(\phi) - R\sin(\theta))^2} \tag{22}$$

$$= \begin{cases} U^i(s,x) = \ln R - \sum\limits_{m=1}^{\infty} \frac{1}{m}\left(\frac{\rho}{R}\right)^m \cos m(\theta - \phi), \\ \qquad\qquad\qquad\qquad\qquad R > \rho \\ U^e(s,x) = \ln\rho - \sum\limits_{m=1}^{\infty} \frac{1}{m}\left(\frac{R}{\rho}\right)^m \cos m(\theta - \phi), \\ \qquad\qquad\qquad\qquad\qquad R < \rho \end{cases} \tag{23}$$

$$L(s,x) = \frac{\partial \ln r}{\partial \rho} = \frac{\rho - R\cos(\phi - \theta)}{R^2 + \rho^2 - 2R\rho\cos(\phi - \theta)} \tag{24}$$

$$= \begin{cases} L^i(s,x) = -\sum\limits_{m=1}^{\infty} \frac{\rho^{m-1}}{R^m}\cos(m(\theta - \phi)), \\ \qquad\qquad\qquad\qquad\qquad R > \rho \\ L^e(s,x) = \frac{1}{\rho} + \sum\limits_{m=1}^{\infty} \frac{R^m}{\rho^{m+1}}\cos(m(\theta - \phi)), \\ \qquad\qquad\qquad\qquad\qquad R < \rho \end{cases} \tag{25}$$

$$T(s,x) = \frac{\partial \ln r}{\partial R} = \frac{R - \rho\cos(\phi - \theta)}{R^2 + \rho^2 - 2R\rho\cos(\phi - \theta)} \tag{26}$$

$$= \begin{cases} T^i(s,x) = \frac{1}{R} + \sum\limits_{m=1}^{\infty} \frac{\rho^m}{R^{m+1}}\cos(m(\theta - \phi)), \\ \qquad\qquad\qquad\qquad\qquad R > \rho \\ T^e(s,x) = -\sum\limits_{m=1}^{\infty} \frac{R^{m-1}}{\rho^m}\cos(m(\theta - \phi)), \\ \qquad\qquad\qquad\qquad\qquad R < \rho \end{cases} \tag{27}$$

$$M(s,x) = \frac{\partial^2 \ln r}{\partial\rho\partial R} = \frac{-2R\rho + (R^2 + \rho^2)\cos(\theta - \phi)}{(R^2 + \rho^2 - 2R\rho\cos(\theta - \phi))^2} \tag{28}$$

$$= \begin{cases} M^i(s,x) = \sum\limits_{m=1}^{\infty} \frac{m\rho^{m-1}}{R^{m+1}}\cos(m(\theta - \phi)), \\ \qquad\qquad\qquad\qquad\qquad R > \rho \\ M^e(s,x) = \sum\limits_{m=1}^{\infty} \frac{mR^{m-1}}{\rho^{m+1}}\cos(m(\theta - \phi)), \\ \qquad\qquad\qquad\qquad\qquad R < \rho \end{cases} \tag{29}$$

where $s = (R, \theta)$ and $x = (\rho, \phi)$ in the polar coordinate.

We can find the following relations between the interior and exterior kernels from Eqs. (22)$\sim$(28), as shown below:

$$U_{ij}^E = U_{ij}^I \quad \text{or} \quad U^E(s,x) = U^I(s,x) \tag{30}$$
$$T_{ij}^E = L_{ij}^I \quad \text{or} \quad T^E(s,x) = L^I(s,x) \tag{31}$$
$$L_{ij}^E = T_{ij}^I \quad \text{or} \quad L^E(s,x) = T^I(s,x) \tag{32}$$
$$M_{ij}^E = M_{ij}^I \quad \text{or} \quad M^E(s,x) = M^I(s,x). \tag{33}$$

Since the rotation symmetry is preserved for a circular boundary, the four influence matrices in Eqs. (13)$\sim$(16) are the circulants with the elements

$$K_{ij} = K(R, \theta_j, \rho, \phi_i) \tag{34}$$

where the kernel K can be U, T, L or M in Eqs. (13)$\sim$(16), ϕ_i and θ_j are the angles of collocation and source points, respectively. By superimposing $2N$ lumped strength along the boundary, we have the influence matrices,

$$[K] = \begin{bmatrix} k_0 & k_1 & \cdots & k_{2N-2} & k_{2N-1} \\ k_{2N-1} & k_0 & \cdots & k_{2N-3} & k_{2N-2} \\ k_{2N-2} & k_{2N-1} & \cdots & k_{2N-4} & k_{2N-3} \\ \vdots & \vdots & \ddots & \vdots & \vdots \\ k_1 & k_2 & \cdots & k_{2N-1} & k_0 \end{bmatrix} \tag{35}$$

where the elements of the first row can be obtained by

$$K_j = K(R, \theta_j, \rho, 0) \tag{36}$$

in which $\phi = 0$ without loss of generality. The matrix $[K]$ in Eq.(35) is found to be a circulant (Chen *et al.* 2000) since the rotational symmetry for the influence coefficients is considered. By introducing the following bases for the circulants, I, $(C_{2N})^1$, $(C_{2N})^2$, ..., and $(C_{2N})^{2N-1}$, we can expand $[K]$ into

$$[K] = k_0 I + k_1(C_{2N})^1 + k_2(C_{2N})^2 + \cdots + k_{2N-1}(C_{2N})^{2N-1}, \tag{37}$$

where I is an identity matrix and

$$C_{2N} = \begin{bmatrix} 0 & 1 & \cdots & 0 & 0 \\ 0 & 0 & \cdots & 0 & 0 \\ \vdots & \vdots & \ddots & \vdots & \vdots \\ 0 & 0 & \cdots & 0 & 1 \\ 1 & 0 & \cdots & 0 & 0 \end{bmatrix}_{2N \times 2N} . \quad (38)$$

Based on the circulant theory, the eigenvalues for the influence matrix, $[K]$, are found as follows:

$$\lambda_l = k_0 + k_1 \alpha_l + k_2 \alpha_l^2 + \cdots + k_{2N-1} \alpha_l^{2N-1}$$
$$l = 0, \pm 1, \pm 2, \cdots, \pm(N-1), N \quad (39)$$

where λ_l and α_l are the eigenvalues for $[K]$ and $[C_{2N}]$, respectively. It is easily found that the eigenvalues for the circulant $[C_{2N}]$ are the roots for $\alpha^{2N} = 1$ as shown below:

$$\alpha_l = e^{i\frac{2\pi l}{2N}},$$
$$l = 0, \pm 1, \pm 2, \cdots, \pm(N-1), N \text{ or} \quad (40)$$
$$l = 0, 1, 2, \cdots, 2N-1.$$

Substituting Eq.(40) into Eq.(39), we have

$$\lambda_l = \sum_{m=0}^{2N-1} k_m \alpha_l^m = \sum_{m=0}^{2N-1} k_m e^{i\frac{2\pi}{2N}ml},$$
$$l = 0, \pm 1, \pm 2, \cdots, \pm(N-1), N. \quad (41)$$

According to the definition for k_m in Eq.(36), we have

$$k_m = k_{2N-m}, \quad m = 0, 1, 2, \cdots, 2N-1. \quad (42)$$

Substitution of Eq.(42) into Eq.(41) yields

$$\lambda_l = k_0 + (-1)^l k_N + \sum_{m=1}^{N-1} (\alpha_l^m + \alpha_l^{2N-m}) k_m$$
$$= \sum_{m=0}^{2N-1} \cos(ml\Delta\theta) k_m. \quad (43)$$

Substituting Eq. (23) into Eq. (43) for U matrix by setting $\phi = 0$ without loss of generality, the Riemann sum of infinite terms reduces to the following integral

$$\lambda_l = \frac{1}{\Delta\theta} \lim_{N \to \infty} \sum_{m=0}^{2N-1} \cos(ml\Delta\theta) U(m\Delta\theta, 0)\Delta\theta \quad (44)$$

$$\approx \frac{2N}{2\pi} \int_0^{2\pi} \cos(l\theta) U(\theta, 0) d\theta, \quad (45)$$

where $\Delta\theta = 2\pi/2N$.

(i) Interior problem

By using the degenerate kernel $U^i(s,x)$ for interior problem $(R > \rho)$ in Eq. (23) and the orthogonal conditions, Eq. (45) reduces to

$$\lambda_l^i = \begin{cases} 2N \ln R, & l = 0 \\ -N/|l|, & l = \pm 1, \pm 2, \cdots, \pm(N-1), N \end{cases} \quad (46)$$

Similarly, we have

$$\mu_l^i = \begin{cases} 0, & l = 0 \\ -N/R, & l = \pm 1, \pm 2, \cdots, \pm(N-1), N \end{cases} \quad (47)$$

$$v_l^i = \begin{cases} 2N/R, & l = 0 \\ N/R, & l = \pm 1, \pm 2, \cdots, \pm(N-1), N \end{cases} \quad (48)$$

$$\delta_l^i = \begin{cases} 0, & l = 0 \\ N|l|/R^2, & l = \pm 1, \pm 2, \cdots, \pm(N-1), N \end{cases} \quad (49)$$

where μ_l^i, v_l^i and δ_l^i are the eigenvalues of $[L^i]$, $[T^i]$ and $[M^i]$ matrices, respectively. Using the invariant property for the influence matrices, the first invariant is the sum of all the eigenvalues. The diagonal coefficients for the four matrices are obtained by adding all the eigenvalues and can be shown below:

$$2Na_{jj} = \sum_{m=0}^{2N-1} \lambda_m^i, (j \ no \ sum) \quad (50)$$

$$2Nb_{jj} = \sum_{m=0}^{2N-1} \mu_m^i, \quad (51)$$

$$2Nc_{jj} = \sum_{m=0}^{2N-1} v_m^i, \quad (52)$$

$$2Nd_{jj} = \sum_{m=0}^{2N-1} \delta_m^i. \quad (53)$$

Hence, the diagonal elements are easily deter-

mined from the first invariant as follows:

$$a_{jj} = \ln R - [2(\frac{1}{1} + \frac{1}{2} + \cdots + \frac{1}{N-1}) + \frac{1}{N}], \quad (54)$$

$$b_{jj} = \frac{1-2N}{2R} \approx \frac{-\pi}{2\pi R/2N}, \quad N \gg 1, \quad (55)$$

$$c_{jj} = \frac{1+2N}{2R} \approx \frac{\pi}{2\pi R/2N}, \quad N \gg 1, \quad (56)$$

$$d_{jj} = \frac{1}{R^2}[1 + 2 + \cdots + (N-1) + N]. \quad (57)$$

(ii) Exterior problem

By using the degenerate kernel $U^e(s,x)$ for exterior problem ($R < \rho$) in Eq. (23) and the orthogonal conditions, Eq.(45) reduces to

$$\lambda_l^e = \begin{cases} 2N \ln R, & l = 0 \\ -N/|l|, & l = \pm 1, \pm 2, \cdots, \pm(N-1), N \end{cases} \quad (58)$$

Similarly, we have

$$\mu_l^e = \begin{cases} -2N/R, & l = 0 \\ -N/R, & l = \pm 1, \pm 2, \cdots, \pm(N-1), N \end{cases} \quad (59)$$

$$v_l^e = \begin{cases} 0, & l = 0 \\ N/R, & l = \pm 1, \pm 2, \cdots, \pm(N-1), N \end{cases} \quad (60)$$

$$\delta_l^e = \begin{cases} 0, & l = 0 \\ N|l|/R^2, & l = \pm 1, \pm 2, \cdots, \pm(N-1), N \end{cases} \quad (61)$$

where μ_l^e, v_l^e and δ_l^e are the eigenvalues of $[L^e]$, $[T^e]$ and $[M^e]$ matrices, respectively. Using the invariant property for the influence matrices, the first invariant is the sum of all the eigenvalues. The diagonal coefficients for the four matrices are obtained by adding all the eigenvalues and can be

shown below:

$$2Na_{jj} = \sum_{m=0}^{2N-1} \lambda_m^e, \quad (62)$$

$$2Nb_{jj} = \sum_{m=0}^{2N-1} \mu_m^e, \quad (63)$$

$$2Nc_{jj} = \sum_{m=0}^{2N-1} v_m^e, \quad (64)$$

$$2Nd_{jj} = \sum_{m=0}^{2N-1} \delta_m^e. \quad (65)$$

Hence, the diagonal elements are easily determined from the first invariant as follows:

$$a_{jj} = \ln R - [2(\frac{1}{1} + \frac{1}{2} + \cdots + \frac{1}{N-1}) + \frac{1}{N}], \quad (66)$$
$$(j \text{ no sum})$$

$$b_{jj} = \frac{-(1+2N)}{2R} \approx \frac{-\pi}{2\pi R/2N}, \quad N \gg 1, \quad (67)$$

$$c_{jj} = \frac{-(1-2N)}{2R} \approx \frac{\pi}{2\pi R/2N}, \quad N \gg 1, \quad (68)$$

$$d_{jj} = \frac{1}{R^2}[1 + 2 + \cdots + (N-1) + N]. \quad (69)$$

The properties for the influence matrices are shown in Table 1.

4 Derivation of diagonal coefficients of influence matrices with arbitrary domain for the MMFS

The finite value of the diagonal terms of the influence matrices for the MMFS can be extracted out by the analog of Eq. (21) between the MMFS and the indirect BEM (Chen & Hong 1992) on an *ad hoc* concept.

4.1 Interior problem

By employing the regularized technique for singular element (Cauchy principal value and Hadamard principal value) in the indirect BEM, the explicit form of diagonal coefficients in the four influence matrices of the indirect BEM can be derived. From the relation between the MMFS and the indirect BEM in Eq. (21), the diagonal coefficients in the four influence matrices of the

MMFS can be shown below:

$$a_{ii} = \frac{[v\ln|v| - v]}{0.5(l_{i,i-1}+l_{i,i+1})}\bigg|_{-0.5l_{i,i-1}}^{0.5l_{i,i+1}}, \tag{70}$$

$$b_{ii} = \frac{-\pi}{0.5(l_{i,i-1}+l_{i,i+1})}, \tag{71}$$

$$c_{ii} = \frac{\pi}{0.5(l_{i,i-1}+l_{i,i+1})}, \tag{72}$$

$$d_{ii} = \frac{1}{v0.5(l_{i,i-1}+l_{i,i+1})}\bigg|_{-0.5l_{i,i-1}}^{0.5l_{i,i+1}} \tag{73}$$

where $l_{i,i-1}$ is the distance between the $(i-1)$th source point and the ith source point.

4.2 Exterior problem

According to the dependence of the outward normal vector in the four kernel functions of the MMFS for the interior and exterior problems, the diagonal coefficients of the four influence matrices are the same for the interior and exterior problems. The diagonal terms of the influence matrices in the MMFS using the analytical method and the approximate method are shown in Table 1. The *UL* method of the MMFS is adopted here for solving the below four numerical examples.

5 Numerical examples

To demonstrate the validity of the MMFS, four examples for the interior and exterior Laplace problems subject to the various types of B.Cs. are given. The real physical problems for the Laplace equation contain potential flow problems, torsion bar problem, Stokes equations of the vorticity transport equation in the scalar form *etc*. In case 1, the interior problems for circular domain subject to the Neumman B. C. are discussed. In case 2, we deal with the exterior problems for circular domain subjected to the discontinuous Dirichlet B. C. In case 3, the square geometry with discontinuous Dirichlet B. C. is considered. In case 4, we demonstrate the ability of the MMFS to solve the water wave problem with infinite strip domain of normal incident water wave past a submerged breakwater. The governing equation considered is the Laplace equation.

Table 1: The properties of the influence matrices for the Laplace equation.

	$U(s,x)=\ln r$		$L(s,x)=\dfrac{\partial U(s,x)}{\partial n_x}=\dfrac{y_i\bar n_i}{r^2}$		$T(s,x)=\dfrac{\partial U(s,x)}{\partial n_s}=\dfrac{-y_i\bar n_i}{r^2}$		$M(s,x)=\dfrac{\partial^2 U(s,x)}{\partial n_s\partial n_x}=\dfrac{2y_iy_j\bar n_i\bar n_j}{r^4}-\dfrac{n_i\bar n_i}{r^2}$	
Kernel function	Exterior	Interior	Exterior	Interior	Exterior	Interior	Exterior	Interior
Eigenvalue λ_i	$\lambda_0^e=2N\ln R$, $\lambda_i^e=-\frac{N}{i}$	$\lambda_0^i=2N\ln R$, $\lambda_i^i=-\frac{N}{i}$	$\lambda_0^e=-\frac{2N}{R}$, $\lambda_i^e=-\frac{N}{R}$	$\lambda_0^i=0$, $\lambda_i^i=-\frac{N}{R}$	$\lambda_0^e=0$, $\lambda_i^e=\frac{N}{R}$	$\lambda_0^i=\frac{2N}{R}$, $\lambda_i^i=\frac{N}{R}$	$\lambda_0^e=0$, $\lambda_i^e=\frac{N}{R^2}$	$\lambda_0^i=0$, $\lambda_i^i=\frac{N}{R^2}$
Diagonal value	$\ln R-[2(\frac{1}{1}+\frac{2}{1}+\ldots+\frac{1}{N-1})+\frac{1}{N}]$	$\ln R-[2(\frac{1}{1}+\frac{2}{1}+\ldots+\frac{1}{N-1})+\frac{1}{N}]$	$-\frac{N}{R}-\frac{1}{2R}$	$-\frac{N}{R}+\frac{1}{2R}$	$\frac{N}{R}-\frac{1}{2R}$	$\frac{N}{R}+\frac{1}{2R}$	$\frac{\pi}{R^2}[1+2+\ldots+(N-1)+N]$	$\frac{\pi}{R^2}[1+2+\ldots+(N-1)+N]$
	$v\log\lvert v\rvert\big|_{-0.5l_{i,i-1}}^{0.5l_{i,i+1}}$	$v\log\lvert v\rvert\big|_{-0.5l_{i,i-1}}^{0.5l_{i,i+1}}$	$\frac{-\pi}{0.5(l_{i,i-1}+l_{i,i+1})}$	$\frac{-\pi}{0.5(l_{i,i-1}+l_{i,i+1})}$	$\frac{\pi}{0.5(l_{i,i-1}+l_{i,i+1})}$	$\frac{\pi}{0.5(l_{i,i-1}+l_{i,i+1})}$	$\frac{\pi}{0.5v(l_{i,i-1}+l_{i,i+1})}\big|_{-0.5l_{i,i-1}}^{0.5l_{i,i+1}}$	$\frac{\pi}{0.5v(l_{i,i-1}+l_{i,i+1})}\big|_{-0.5l_{i,i-1}}^{0.5l_{i,i+1}}$

$$\frac{1}{2N}\sum_{m=0}^{2N}\lambda_m = \frac{\text{Sum of diagonal terms}}{2N}\quad\text{(circular domain only)}$$

Approximate solution (arbitrary domain)

Here $r=|x-s|$, $y_i = x_i - s_i$, $\bar n_i$ denotes the ith components of normal vector on x, respectively.
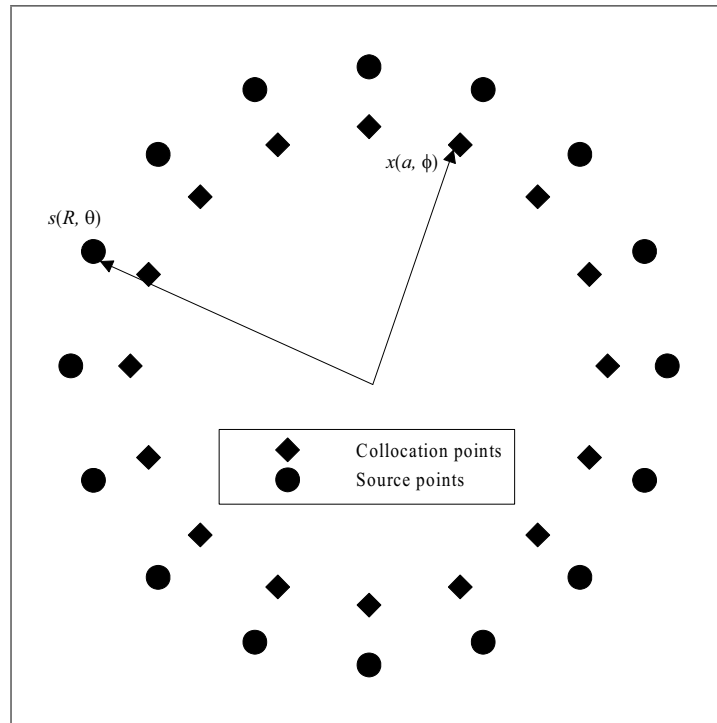
(a) Conventional MFS
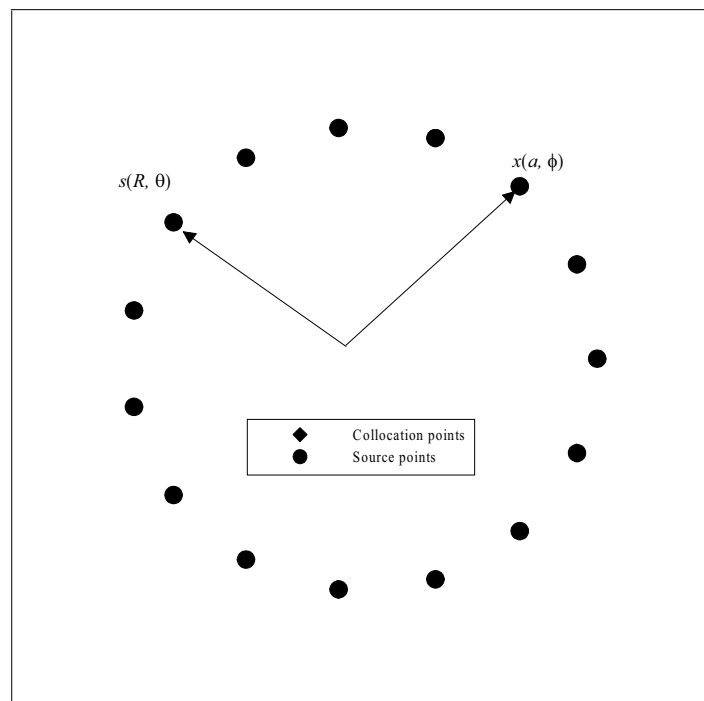
(b) MMFS

Figure 1: The sketch of node distribution for the interior problem with circular domain in the case 1 (a) Conventional MFS, (b) MMFS.

Case 1: Interior problem with a circular domain subject to the Neumann B. C.

A circular domain ($a = 2m$) subject to the Neumann B. C. ($t = a^5 \cos(6\phi)$) is considered. The sketch of node distribution using the different methods is plotted in Fig.1.

In this case, an analytical solution is available as follows:

$$u(\rho, \phi) = \frac{\rho^6}{6} \cos(6\phi), \quad 0 \le \rho \le a, \quad 0 \le \phi < 2\pi \tag{74}$$

The results on the real boundary ($\rho = 2m$) by using the conventional MFS for different off-set distances to boundary, are obtained in Fig.2.

There are non-unique solutions by using the MFS in Fig. 2(a) and (b) for $\rho = 2m$ and $\rho = 1m$, respectively. To deal with the non-unique problem, the rigid body terms are added in the solutions to constrain the potential in the origin point to be zero. Therefore, we can shift the solution to the exact solution as shown in Fig.3 (a) and (b). It is obvious that the relative errors of the conventional MFS comparing with the exact solution for $R = 2.1m$ and $R = 50m$ are larger than that of $R = 3m$ from Fig.3 (a) and (b).

This means that the location of source points is very important to the accuracy of the solution by using the conventional MFS. The results by using the MMFS and the conventional MFS ($R = 3m$) are plotted in Fig.4 (a) and (b).

Fig.4 (a) and (b) show the convergence of the solution using the MMFS. The field solutions by using the two MFS and the exact solution are plotted in Fig.5 (a)~(c).

Case 2: Exterior problem with a circular domain subject to the discontinuous Dirichlet B. C.

A circular domain ($a = 1m$) subject to the discontinuous Dirichlet B. C. is given as follows:

$$u(a, \phi) = \begin{cases} 1, & 0 < \phi < \pi, \\ -1, & \pi < \phi < 2\pi. \end{cases} \tag{75}$$

The sketch of node distribution using the different methods is plotted in Fig.6.

The exact solution is available as

$$u(x, y) = \frac{2}{\pi} \tan^{-1}\left(\frac{2y}{x^2 + y^2 - 1}\right). \tag{76}$$

The field potential solution of the exact solution is shown in Fig.7.

We obtain the results of the field potential solution by using the conventional MFS (100 nodes) for different off-set distances to boundary as shown in Fig.8.

The relative errors of the conventional MFS are larger for $R = 0.9999m$ and $R = 0.5m$ than $R = 0.8m$. The field solution of the MMFS is plotted in Fig.9.

The problem of non-unique solutions using the conventional MFS and the MMFS is overcome by superimposing a rigid body term in the fundamental solution to avoid the zero eigenvalue originating from the degenerate scale (Chen *et al.*, 2003). The result matches the exact solution very well by using the MMFS.

Case 3: Interior problem with a square domain subject to the Dirichlet B. C.

A square domain ($1m \times 1m$) subject to the Dirichlet boundary condition is considered as

$$u(x, 0) = x, \quad u(x, 1) = u(0, y) = u(1, y) = 0. \tag{77}$$

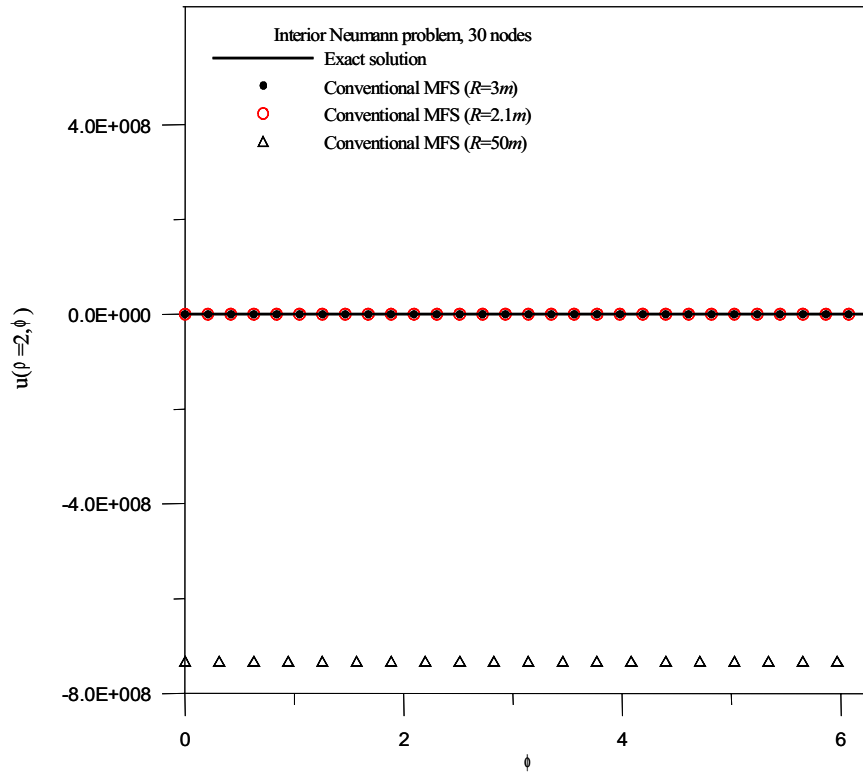In this case, an analytical solution is available as follows:

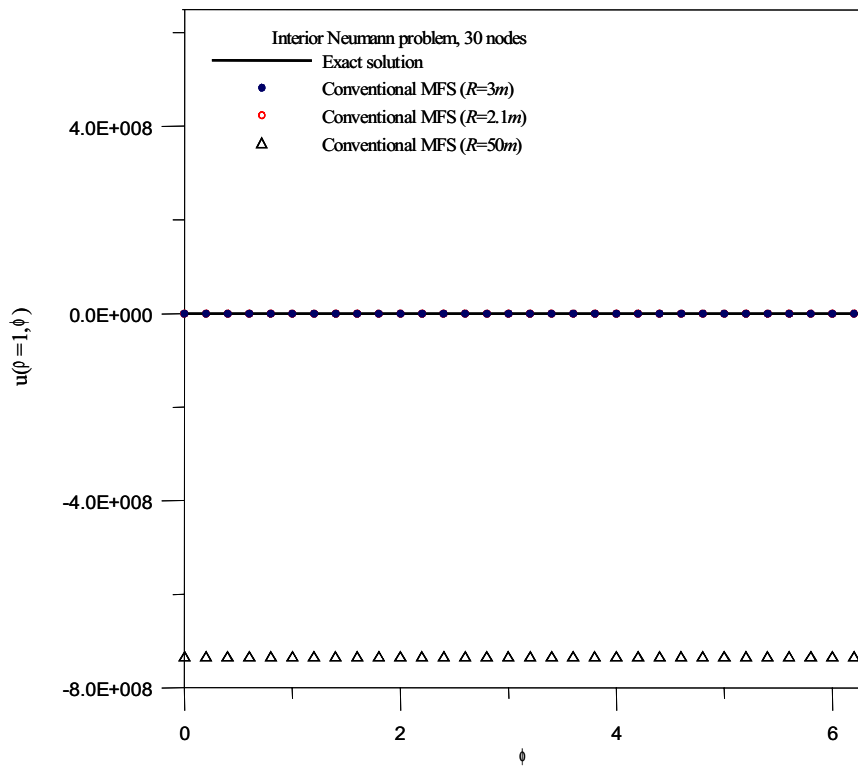$$u(x, y) = \sum_{n=1}^{\infty} C_n \sinh(n\pi(1 - y)) \sin(n\pi x), \tag{78}$$

where

$$C_n = \frac{2}{\sinh(n\pi)} \int_0^1 x \sin(n\pi x) dx = \frac{2(-1)^{n+1}}{n\pi \sinh n\pi}. \tag{79}$$

The sketch of node distribution using the conventional MFS and MMFS is plotted in Fig.10 (a) and (b), respectively.

To ensure the accuracy of the conventional MFS and the MMFS, the field potential solution of the analytical solution ($n = 200$) is plotted in Fig.11.
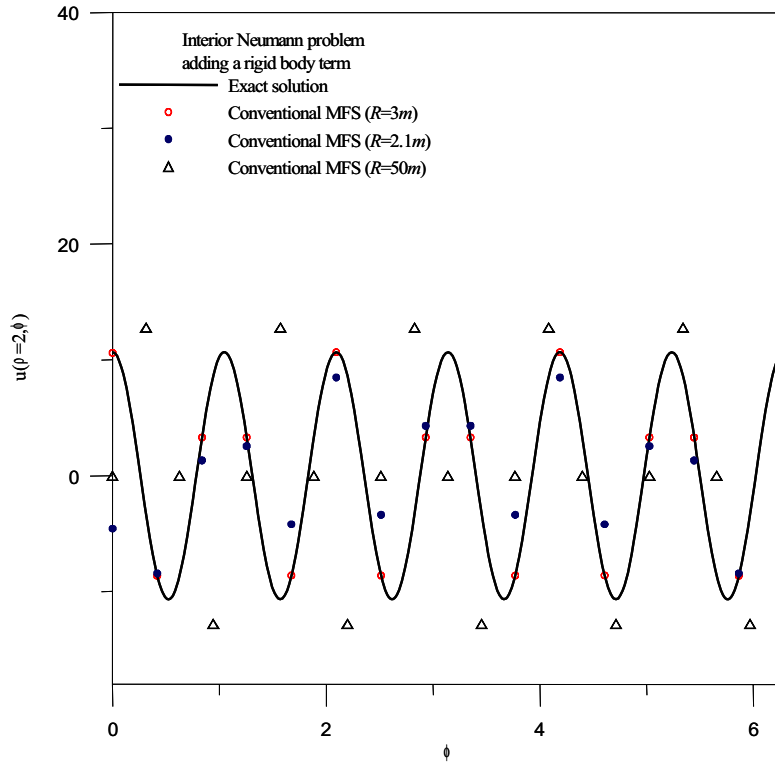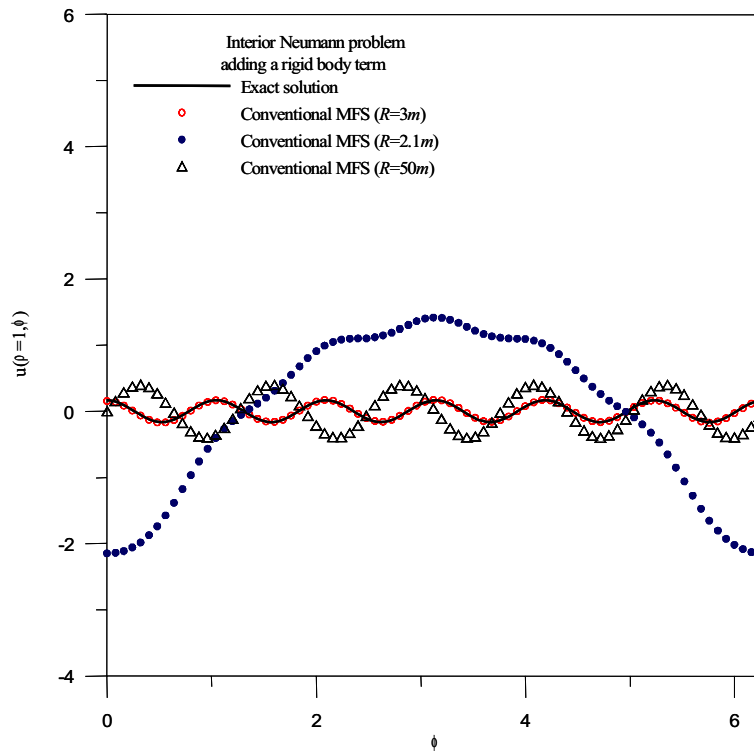
(a) $\rho = 2m$

(b) $\rho = 1m$

Figure 2: The potential solution using the conventional MFS for the case 1, (a) $\rho = 2m$, (b) $\rho = 1m$.

(a) $\rho = 2m$

(b) $\rho = 1m$

Figure 3: The potential solution of the conventional MFS by adding a rigid body term for the case 1, (a) $\rho = 2m$, (b) $\rho = 1m$.
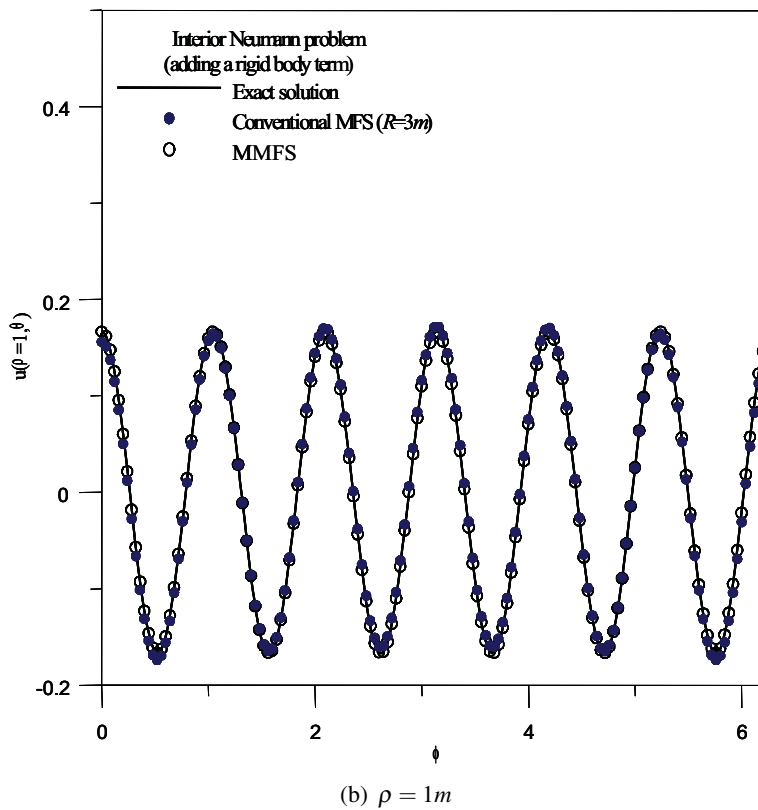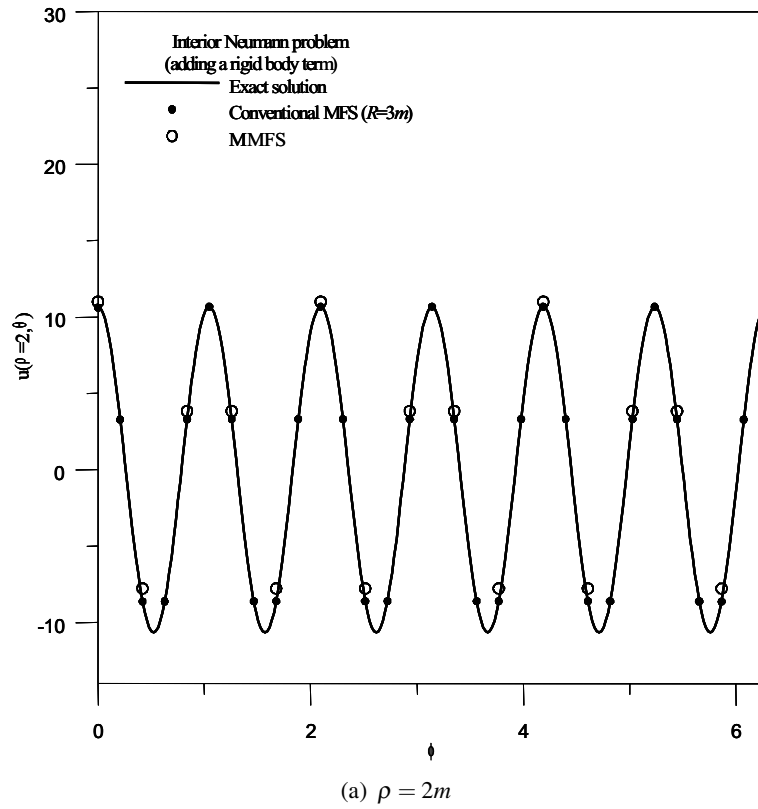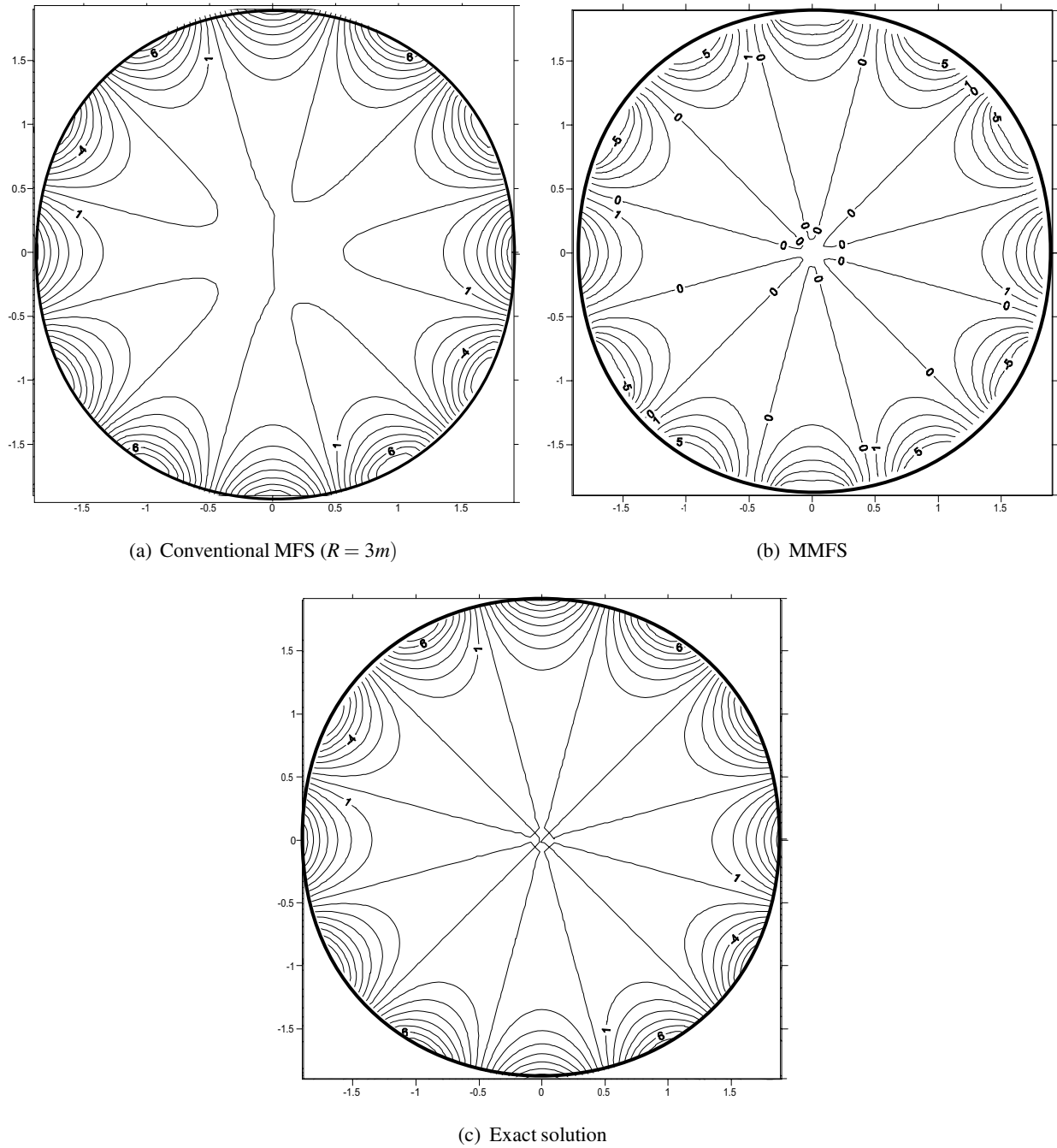
(a) $\rho = 2m$

(b) $\rho = 1m$

Figure 4: The potential solution using the proposed method by adding a rigid body term for the case 1, (a) $\rho = 2m$, (b) $\rho = 1m$.

(a) Conventional MFS ($R = 3m$)

(b) MMFS

(c) Exact solution

Figure 5: The field potential solution for the case 1, (a) Conventional MFS ($R = 3m$), (b) MMFS, (c) Exact solution.
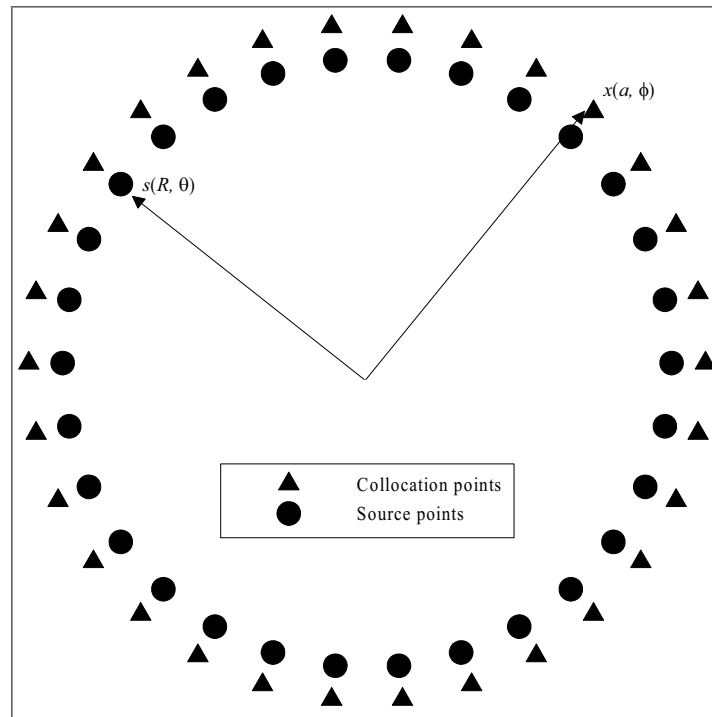
(a) Conventional MFS
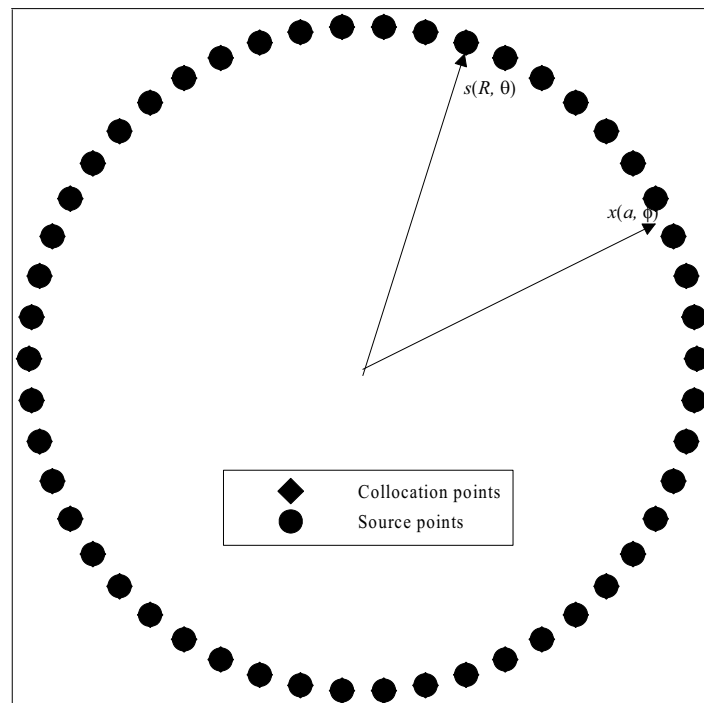
(b) MMFS

Figure 6: The node distribution sketch for exterior problem in the case 2, (a) Conventional MFS, (b) MMFS.
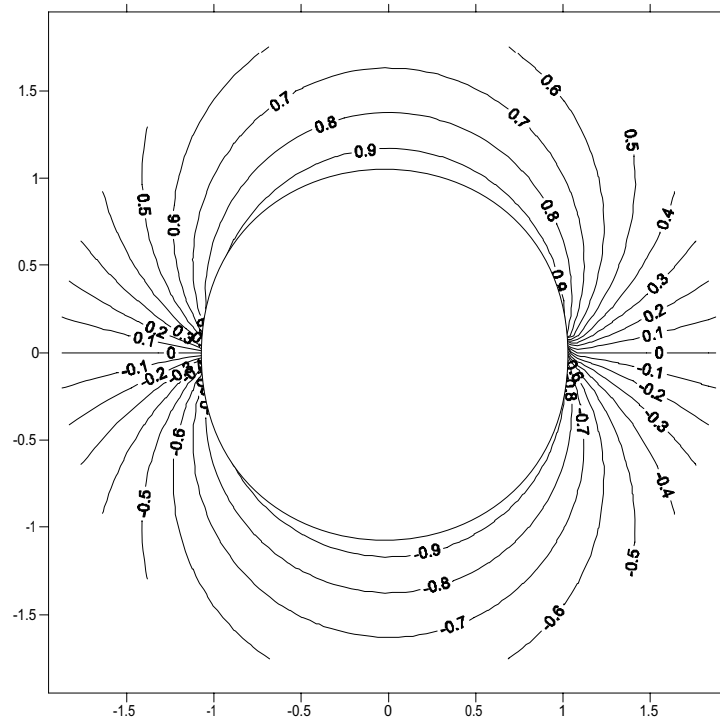
Figure 7: The field potential solution of the exact solution for the case 2.

By collocating eighty nodes, we obtain the results by using the conventional MFS for different off-set distances (*de*) to boundary as depicted in Fig.12

It is obvious that the relative errors of the conventional MFS comparing with the exact solution for *de =0.1m* and *de =1m* are larger than that of *de=0.5m*. This illustrates the fact that the location of source is vital to the accuracy of the solution by using the conventional MFS. The error arises from the kernel's singularity which causes substantial difficulties in solving problems. In such a situation, the conventional MFS does not yield reliable and consistent solutions. The results by using the MMFS are plotted in Fig.13.

It shows the accuracy of the present method after comparing with the analytical solution in Fig.11. Thus the selection of the off-set distances to boundary in the conventional MFS is avoided by adopting the MMFS of the present study.

Case 4: Water wave problem

The water wave problem with a semi-infinite domain of normal incident water wave past a submerged breakwater is considered. An example given by Abul-Azm (1994) with the geometry shown in Fig.14 is solved.

The boundary conditions of the interested domain are summarized as (Chen *et al.* 2002):

1. The linearized free water surface B. C.:

$$\frac{\partial u}{\partial y} - \frac{\sigma^2 u}{g} = 0, \qquad (80)$$

in which g is the acceleration of gravity and σ is the frequency of incident water wave.

2. Seabed and breakwater B. C.:

$$\frac{\partial u}{\partial n} = 0, \qquad (81)$$

where n is boundary normal vector.
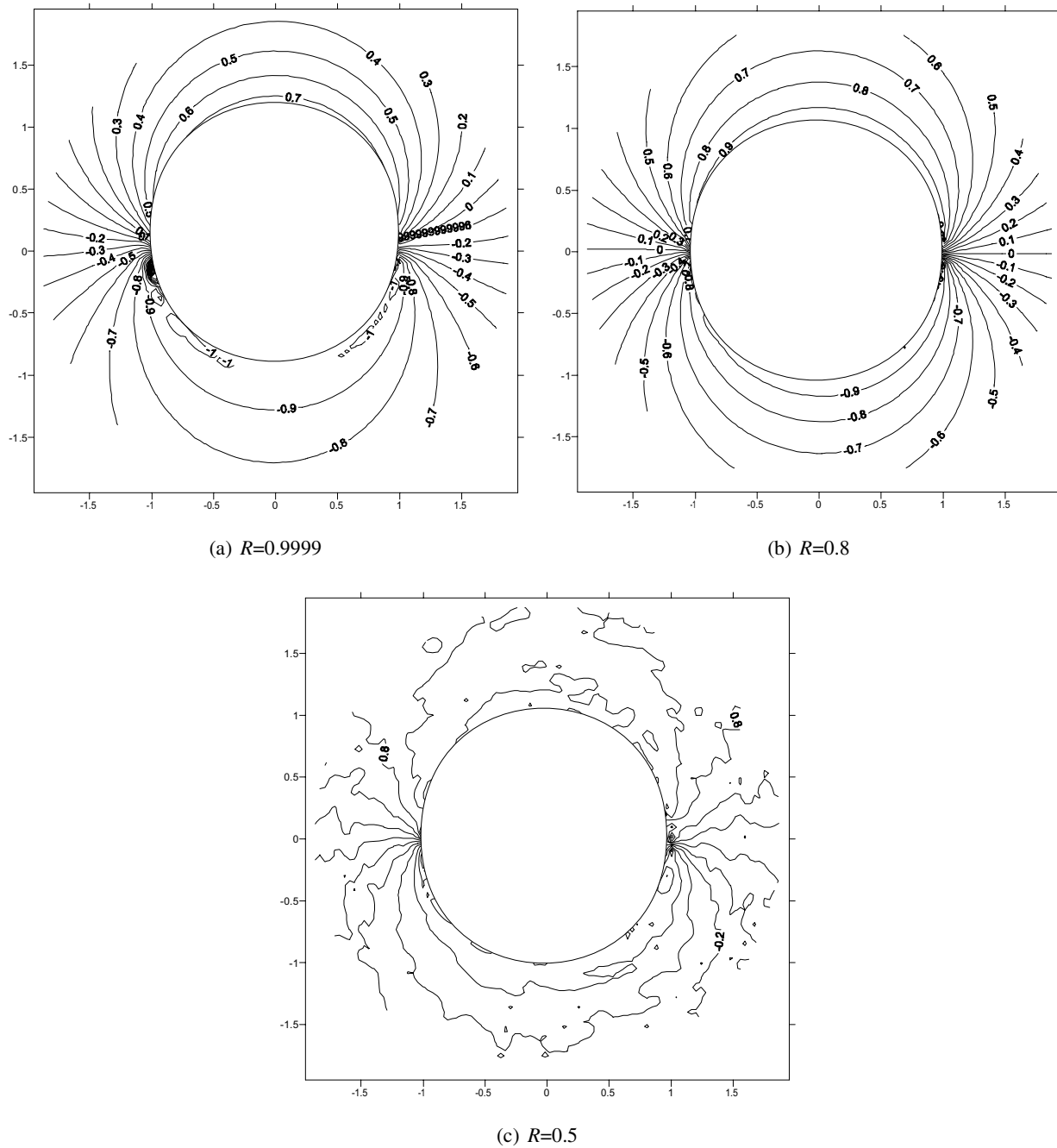
3. The boundary conditions on the fictitious interfaces:

(a) *R*=0.9999

(b) *R*=0.8

(c) *R*=0.5

Figure 8: The field potential solutions of the conventional MFS (100 nodes) by adding a rigid body term for the case 2, (a) *R*=0.9999, (b) *R*=0.8, (c)*R*=0.5.
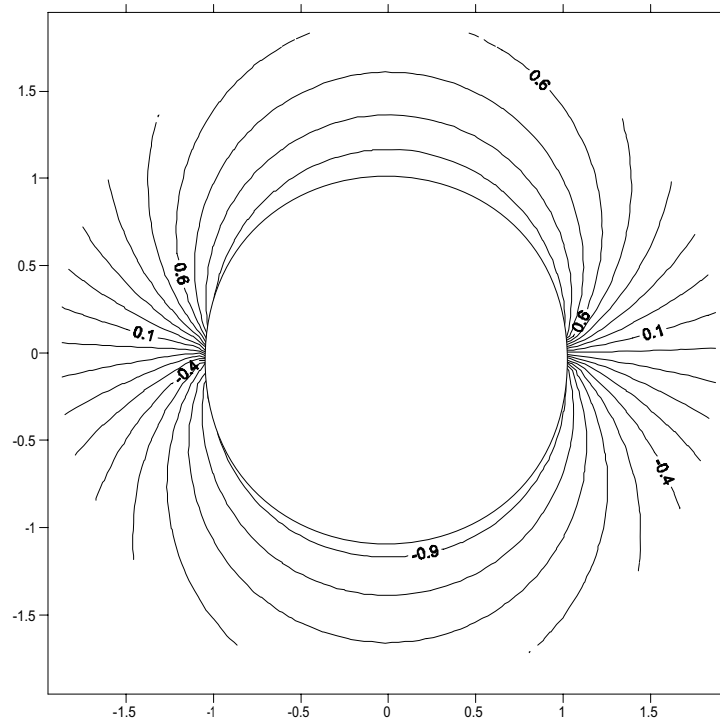
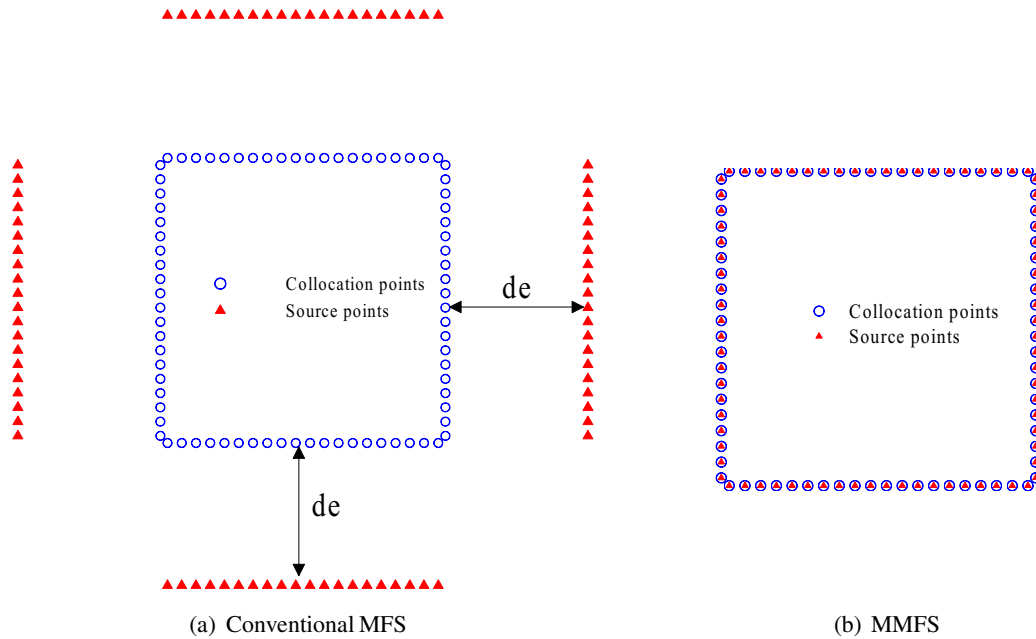Figure 9: The field potential solution of the MMFS (100 nodes) by adding a rigid body term for the case 2.

(a) Conventional MFS   (b) MMFS

Figure 10: The sketch of node distribution (80 nodes) for the case 3, (a) Conventional MFS, (b) MMFS.
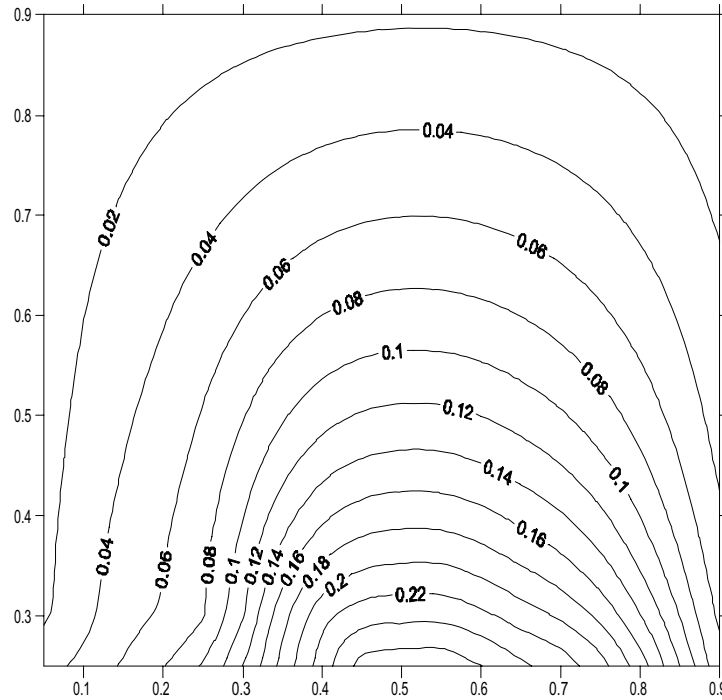
Figure 11: The field potential solution of the exact solution (n=200) for the case 3.

For the infinite strip problem, the domain can be divided into three regions after introducing two pseudo-boundaries on both sides of the barrier, $x = \pm l$, as shown in Fig.14. The potential in the region I without energy loss can be expressed as:

$$u^{(1)}(x,y) = (e^{i\eta(x+l)} + Re^{-i\eta(x+l)})$$
$$\cdot \frac{\cosh(k(h+y))}{\cosh(kh)}, \quad (82)$$

where the superscript of u denotes the region number, k is the wave number which satisfies the dispersion relation, R is the reflection coefficient and $\eta = k\cos(\theta)$. The potential in the region III without energy loss can be expressed as:

$$u^{(3)}(x,y) = Te^{i\eta(x-l)}\frac{\cosh(k(h+y))}{\cosh(kh)}, \quad (83)$$

where T is the transmission coefficient.

The boundary conditions on the fictitious inter-

faces are

$$u^{(1)}(-l,y) = u^{(2)}(-l,y), \quad (84)$$

$$\left.\frac{\partial u^{(1)}}{\partial x}\right|_{x=-l} = \left.\frac{\partial u^{(2)}}{\partial x}\right|_{x=-l}, \quad (85)$$
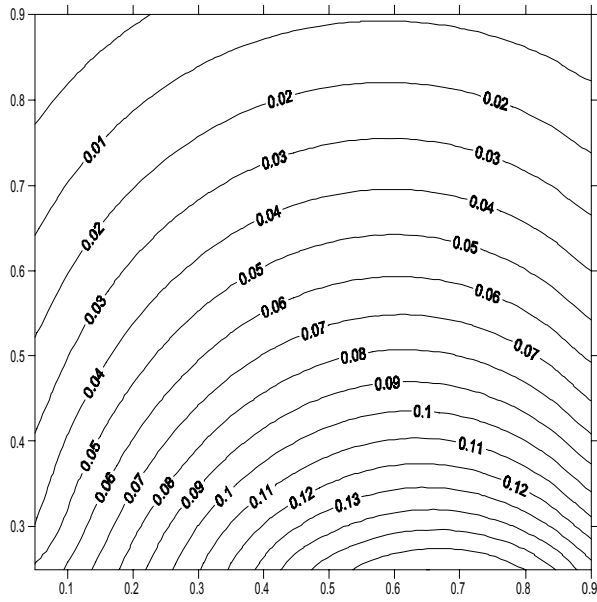
$$u^{(3)}(l,y) = u^{(2)}(l,y), \quad (86)$$

$$\left.\frac{\partial u^{(3)}}{\partial x}\right|_{x=l} = \left.\frac{\partial u^{(2)}}{\partial x}\right|_{x=l}. \quad (87)$$
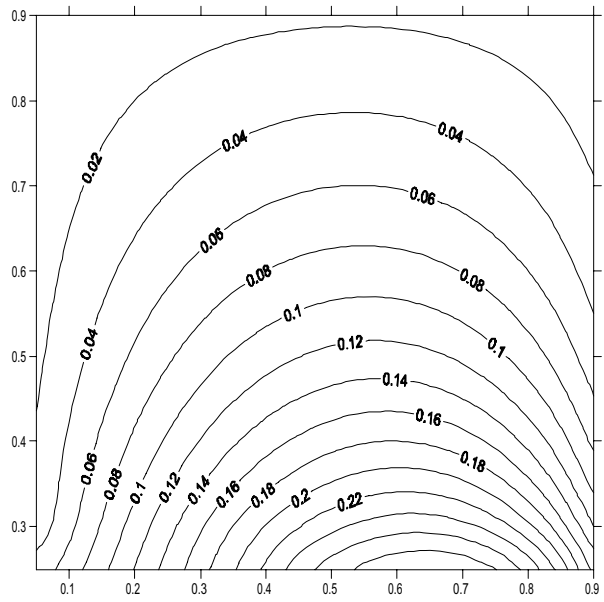
According to Eqs. (82), (83), (84) and (86), we can derive the reflection and transmission coefficients as follows:

$$R =$$
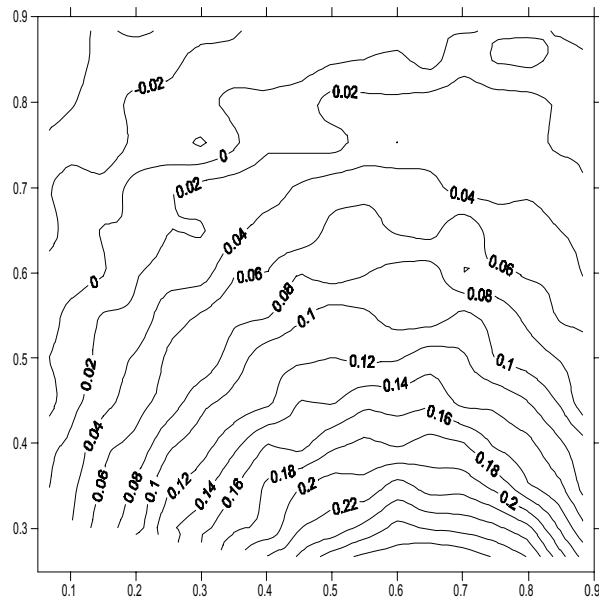$$-1 + \frac{k}{n_0\sinh(kh)}\int_{-h}^{0} u^{(2)}(-l,y)\cosh(k(h+y))dy, \quad (88)$$

$$T = \frac{k}{n_0\sinh(kh)}\int_{-h}^{0} u^{(2)}(l,y)\cosh(k(h+y))dy, \quad (89)$$

(a) *de*=0.1 m

(b) *de*=0.5 m

(c) *de*=1.0 m

Figure 12: The field potential solutions of the conventional MFS (80 nodes) for the case 3, (a) *de*= 0.1 m, (b) *de*= 0.5 m, (c) *de*= 1.0 m.
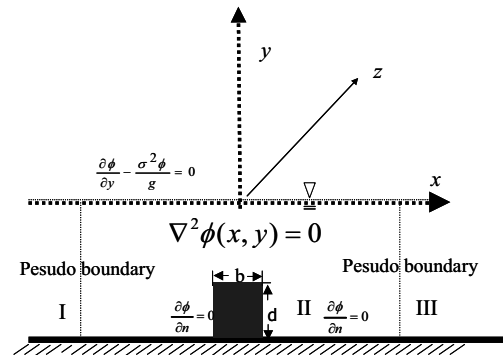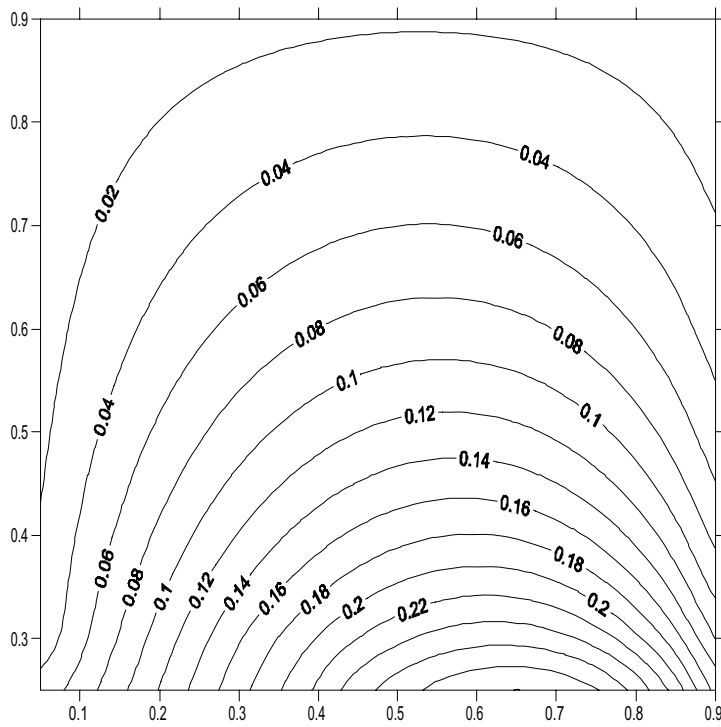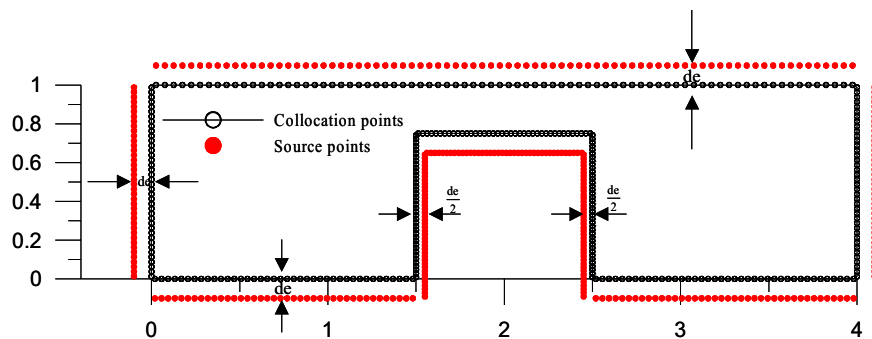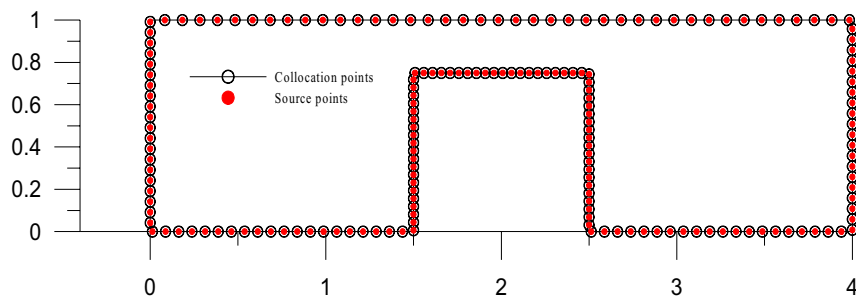
Figure 13: The field potential solution of the MMFS (80 nodes).

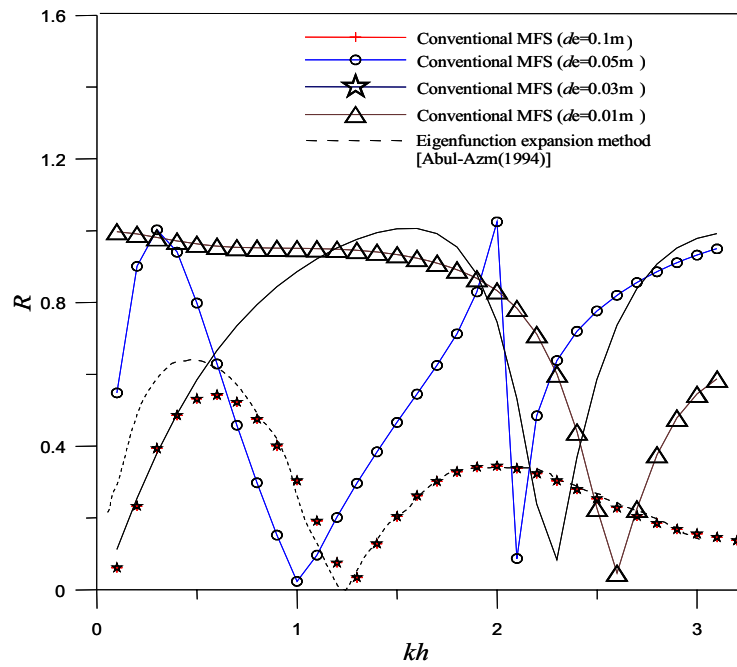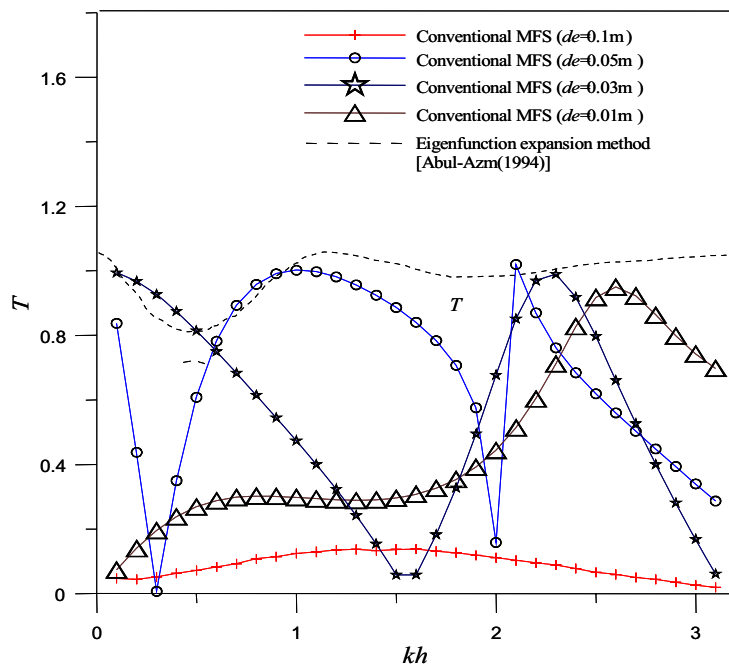Figure 14: Problem sketch of the case 4.

(a) Conventional MFS

(b) MMFS

Figure 15: The sketch of node distribution for the case 4, (a) the conventional MFS, (b) the MMFS.

(a) *R*

(b) *T*

Figure 16: The reflection (*R*) and transmission (*T*) coefficients versus *kh* using the conventional MFS (400 nodes) for the case 4, (a) *R*, (b)*T*.
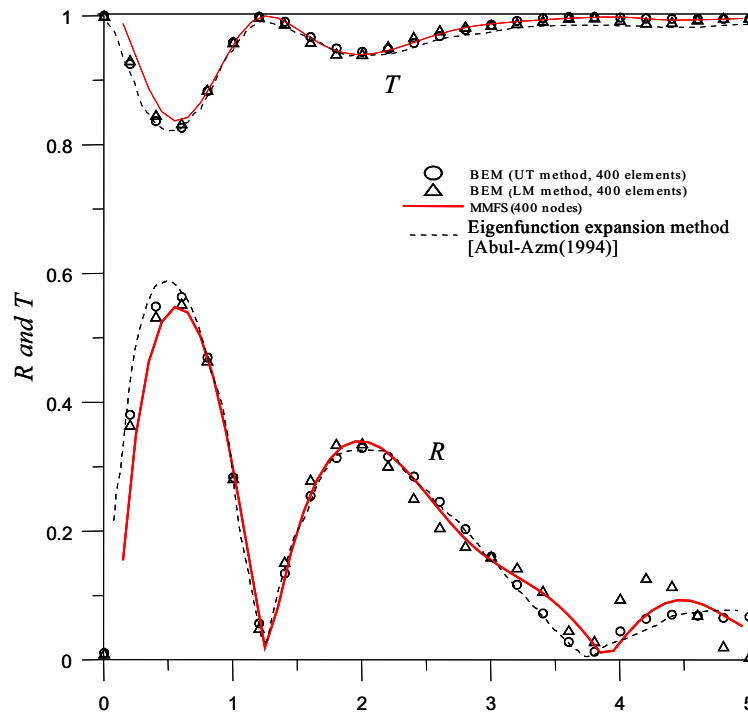
Figure 17: The reflection and transmission coefficients versus *kh* using the MMFS (400 nodes) for the case 4.

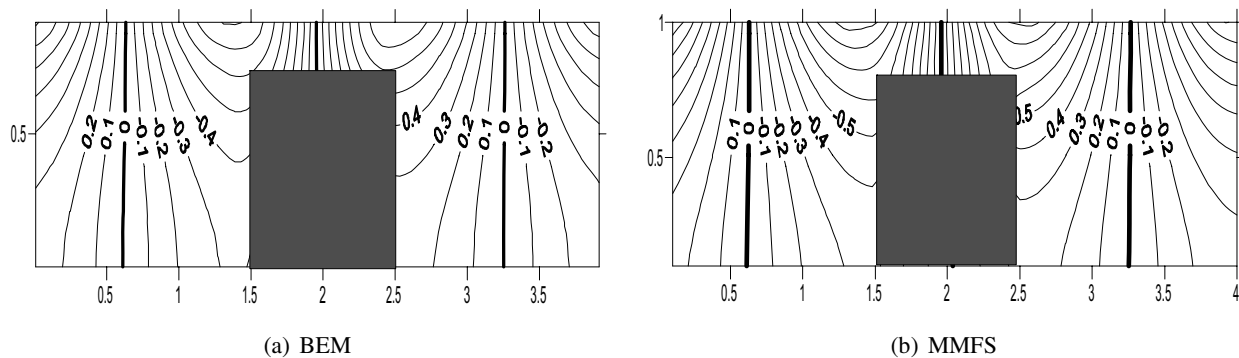(a) BEM   (b) MMFS

Figure 18: The field potential solution (*kh*=2) using the BEM (400 elements) and MMFS (400 nodes) for the case 4, (a) BEM, (b) MMFS.

where $n_0 = \frac{1}{2}\left(1 + \frac{2kh}{\sinh(2kh)}\right)$. The similar B. C. was handled by using the MFS (Balakrishnan & Ramachandran 2000). According to several numerical experiments (Chen *et al.* 2002), the length of each pseudo-boundary (l) is adopted by the double of water depth (h). In this case, the width of the breakwater to water depth ratio (b/h) is 1, and the submergence ratio (D/h) is 0.75. The node distribution for the scattering water wave problem using the conventional MFS and the MMFS is shown in Fig.15 (a) and (b), respectively.

By collocating 400 nodes, the results of the reflection and transmission coefficients by using the conventional MFS for different off-set distances to boundary (*de*), are plotted against *kh* in Fig.16 (a) and (b), respectively.

It is obvious that the results of the conventional MFS for *de*=0.01m, 0.03m, 0.05m and 0.1m are all divergent after comparing with the analytical solution by Abul-Azm (1994). This means that the results fail for different off-set distances to

boundary by using the conventional MFS. The results are plotted in Fig.17.

Fig.17 shows the convergence of the solution using the MMFS. The field potential solution for *kh=2* using the MMFS (400 nodes) and the BEM (400 elements) are shown in Fig.18.

6   Conclusions

In this paper, we proposed a new meshless method (MMFS) to solve the Laplace problems for arbitrary domains subject to the various kinds of B. Cs. Only the boundary nodes on the real boundary are required. It can avoid selecting the off-set distances to boundary in the conventional MFS. Thus the major difficulty of the coincidence of the source and collocation points in the conventional MFS is overcome. Besides, the controversy of the artificial (off-set) boundary outside the physical domain by using the conventional MFS is no longer existent. Although it results in the singularity, the finite values of the diagonal terms for the influence matrices have been extracted out. The ill-posed influence matrices were eliminated when the off-set boundary far from the real boundary is used in the numerical procedures using the conventional MFS. The numerical results were obtained by using the developed program for the four cases of Laplace problems and were compared well with the analytical solutions or other numerical methods.

References

Abramowitz M.; Stegun I. A. (1972): "Handbook of mathematical functions with formulation, graphs and mathematical tables", *Dover, New York.*

Abul-Azm A. G. (1994): "Diffraction through wide submerged breakwaters under oblique wave", *Ocean Engineering*, **21**, 683-706.

Atluri S. N.; Liu H. T.; Han Z. D. (2006):
"Meshless local Petrov-Galerkin (MLPG) mixed collocation method for elasticity problems", *CMES: Computer Modeling in Engineering and Science*, **14**, 141-152.

Balakrishnan K.; Ramachandran P. A. (2000): "The method of fundamental solutions for linear diffusion-reaction equations", *Mathematical and Computer Modelling*, **31**, 221-237.

Belytschko T.; Gu L.; Lu Y. (1994): "Fracture and crack growth by element-free Galerkin methods", *Modelling and Simulation in Materials Science and Engineering*, **2**, 519-534.

Chen C. S.; Golberg M. A.; Hon Y. C. (1998): "The method of fundamental solutions and quasi-Monte-Carlo method for diffusion equations", *International Journal for Numerical Methods in Engineering*, **43,** 1421-1435.

Chen J. T.; Hong H.-K. (1992): "Boundary element method", Second Edition, New World Press, Taipei, Taiwan (in Chinese).

Chen J. T.; Kuo S. R.; Chen K. H.; Cheng Y. C. (2000): "Comments on vibration analysis of arbitrary shaped membranes using non-dimensional dynamic influence function", *Journal of Sound and Vibration*, **235**, 156-171.

Chen J. T.; Chang M. H.; Chen K. H.; Lin S. R. (2002a): "The boundary collocation method with meshless concept for acoustic eigenanalysis of two-dimensional cavities using radial basis function", *Journal of Sound and Vibration*, **257**, 667-711.

Chen, J. T., Chang, M. H.; Chen, K. H. (2002b): "Boundary collocation method for acoustic eigenanalysis of three-dimensional cavities using radial basis function", *Computational Mechanics*, **29**, 392-408.

Chen J. T.; Chen K. H.; Chen C. T. (2002c): "Adaptive boundary element method of time-harmonic exterior acoustic problems in two dimensions", *Computer Methods in Applied Mechanics and Engineering*, **191**, 3331-3345.

Chen J. T.; Wu C. S.; Chen I. L.; Chen K. H. (2007): "On the equivalence of Trefftz method and method of fundamental solutions for Laplace and biharmonic equations", *Computers and Mathematics with Applications*, in Press.

Chen J. T.; Chen I. L.; Chen K. H.; Yeh Y. T.; Lee Y. T. (2004a): "A meshless method for free vibration analysis of circular and rectangular clamped plates using radial basis function", *Engineering Analysis with Boundary Elements*, **28**, 535-545.

Chen J. T.; Chen K. H. (2004b): "Applications of the dual integral formulation in conjunction with fast multipole method in large-scale problems for exterior acoustics", *Engineering Analysis with Boundary Elements*, **28**, 685-709.

Chen K. H.; Chen J. T.; Chou C. R.; Yueh C. Y. (2002): "Dual boundary element analysis of oblique incident wave passing a thin submerged breakwater", *Engineering Analysis with Boundary Elements*, **26**, 917-928.

Chen W.; Tanaka M. (2002): "A meshfree, integration-free and boundary-only RBF technique", *Computers and Mathematics with Applications*, **43**, 379-391.

Chen W.; Hon Y. C. (2003): "Numerical investigation on convergence of boundary knot method in the analysis of homogeneous Helmholtz, modified Helmholtz and convection-diffusion problems", *Computer Methods in Applied Mechanics and Engineering*, **192**, 1859-1875.

Cheng A. H. D.; Young D. L.; Tsai C. C. (2000): "The solution of Poisson's equation by iterative DRBEM using compactly supported, positive definite radial basis function", *Engineering Analysis with Boundary Elements*, **24**, 549-557.

Fairweather G.; Karageophis A. (1998), "The method of fundamental solutions for elliptic boundary value problems", *Advances in Computational Mathematics*, **9**, 69-95.

Gingold R. A.; Maraghan J. J. (1977): "Smoothed particle hydrodynamics: theory and applications to non-spherical stars", *Monthly Notices of the Royal Astronomical Society*, **181**, 375-389.

Hadamard J. (1952): "Lectures on Cauchy's problem in linear partial differential equations", *Dover, New York.*

Kang S. W.; Lee J. M.; Kang Y. J. (1999): "Vibration analysis of arbitrary shaped membranes using non-dimensional dynamic influence func-

tion", *Journal of Sound and Vibration*, **221**, 117-132.

Kang S. W.; Lee J. M. (2000): "Application of free vibration analysis of membranes using the non-dimensional dynamic influence function", *Journal of Sound and Vibration*, **234**, 455-470.

Kita E.; Kamiya N. (1994): "Recent studies on adaptive boundary element methods", *Advances in Engineering Software*, **19**, 21-32.

Liu W. K.; Jun S.; Li S.; Adee J.; Belyschko T. (1995): "Reproducing kernel particle methods for structural dynamics", *International Journal for Numerical Methods in Engineering*, **38**, 1655-1679.

Nishimura N. (2002): "Fast multipole accelerated boundary integral equation methods", *Applied Mechanics Reviews*, **55**, 1-27.

Rokhlin V. (1983): "Rapid solution of classical potential theory", *Journal of Computational Physics*, **60**, 187-207.

Stewart J. R.; Hughes T. J. R. (1997): "*h*-Adaptive Finite Element computation of time-harmonic exterior acoustics problems in two dimension", *Computer Methods in Applied Mechanics and Engineering*, **146**, 65-89.

Tanaka M.; Sladek V.; Sladek J. (1994): "Regularization techniques applied to boundary element methods", *Applied Mechanics Reviews*, **47**, 457-499.

Tsai C. C.; Young D. L.; Cheng A. H. D. (2002): "Meshless BEM for three-dimensional Stokes flows", *CMES: Computer Modeling in Engineering and Science*, **3**, 117-128.

Young D. L.; Ruan J. W. (2005): "Method of fundamental solutions for scattering problems of electromagnetic waves ", *CMES: Computer Modeling in Engineering and Science*, **7**, 223-232.